



Supplement of

The impact of regional-scale upper-mantle heterogeneity on glacial isostatic adjustment in West Antarctica

Erica M. Lucas et al.

Correspondence to: Erica M. Lucas (ericamlucas@gmail.com)

The copyright of individual parts of the supplement might differ from the article licence.

S1 Additional details on constructing the regional-scale viscosity models (REG_P, REG_S)

When inserting the regional seismic models into ANT-20, a ~ 75 km smoothing band is adopted along the edges of the regional and continental models to ensure a gradual transition between the models (Fig. 1). The relative travel-time tomography approach adopted by Lucas et al. (2020) provides velocity anomalies relative to an unknown background mean rather than absolute velocities. In contrast, mantle velocity anomalies in ANT-20 are reported relative to the 1-D Earth model STW105 (Kustowski et al., 2008). Consequently, a 0% velocity anomaly in the Lucas et al. (2020) regional seismic models does not correspond to a 0% velocity anomaly in the ANT-20 model. To ensure consistency amongst the regional-scale viscosity models and the CONT viscosity model, we use the maximum and minimum viscosity bounds from the CONT viscosity model as a guide for constructing the regional viscosity models, ensuring upper mantle viscosities in the regional models remain within these viscosity bounds for central West Antarctica.

To evaluate the impact of inserting the regional seismic tomography models into the ANT-20 model over different depth extents, a series of simulations are performed that adopt viscosity models where the regional models are inserted into the continental base model between the base of the lithosphere and either 200 km or 300 km depth (Fig. S2). Up to $\sim 5\%$ difference is found between these simulations and those in which the regional seismic tomography models are inserted to 250 km depth, indicating that the depth extent over which the regional models are inserted into the ANT-20 model has a relatively minor impact on overall GIA model predictions (Fig. S2).

Due to regularization used in the tomographic inversion, seismic velocity anomaly magnitudes are underestimated in the Lucas et al. (2020) models. Using the synthetic checkerboard resolution tests, Lucas et al. (2020) estimates both low- and high-end amplitude recovery values for the P- and S-wave models. Velocity amplitudes recovered in the P- and S-wave models range from ~ 20 - 30% and ~ 15 - 25% , respectively. To further clarify, this means that a 1.0% P-wave velocity anomaly in the seismic velocity model, for example, would correspond to a 3.3% - 5% P-wave velocity anomaly in the mantle. Throughout this study we will discuss results from simulations that adopt regional Earth viscosity models constructed assuming low-end amplitude recovery (i.e., $\sim 20\%$ amplitude recovery for P-wave model and $\sim 15\%$ for S-wave model). The viscosity models are constructed by first scaling the P-wave and S-wave models for low-end amplitude recovery

and then patching the scaled models into the composite ANT-20 and GLAD-M25 global seismic model. We note that the P-wave model of Lucas et al. (2020) is converted to shear-wave velocity anomalies prior to being inserted into the composite model. A simple conversion, where $\frac{\partial \ln(V_P)}{\partial \ln(V_S)} = 0.4$, is employed to convert P-wave velocity anomalies to S-wave velocity anomalies (Antolik et al., 2003). A scaling factor of $0.033^\circ \text{ C}^{-1}$ is used in the conversion of temperature to viscosity for both the REG_P and REG_S models. To assess the impact of accounting for low-end versus high-end amplitude recovery in the body-wave models, we compare results from simulations with Earth models constructed assuming high-end amplitude recovery (i.e., 30% amplitude recovery for P-wave model and $\sim 25\%$ for S-wave model) with simulations adopting REG_P and REG_S in Fig. S3. A similar spatial pattern of GIA predictions, albeit with up to $\sim 7\%$ difference, is found between simulations adopting viscosity models constructed assuming high-end versus low-end amplitude recovery (see Fig. S3 and caption for details).

S2 Comparison of GIA model predictions for simulations adopting ICE-125 versus ICE-25

Several studies investigating GIA in central West Antarctica have adopted 25-year ice histories to model the viscoelastic response of the solid Earth to contemporary ice mass changes (e.g., Powell et al., 2020; Wan et al., 2022; Powell et al., 2022). With upper mantle viscosities suggested in the literature ranging from $\sim 4 \times 10^{18} \text{ Pa s}$ up to 10^{20} Pa s in central West Antarctica (e.g., Nield et al., 2014; Barletta et al., 2018; Ivins et al., 2023), viscous effects are expected to be significant on decadal to centennial timescale (Hay et al., 2017; Kachuck et al., 2020; Wan et al., 2022). Therefore, a 25-year ice history may not be long enough to capture the entire viscous response to contemporary ice mass change. Figure S7 shows the differences in predicted relative sea level and geoid changes over the last 25 years and current crustal motions between simulations adopting the ICE-125 and ICE-25 ice models for all viscosity models considered. Because the ICE-125 and ICE-25 models adopt the same ice loading history for 1992–2017, Figure S7 represents the impact of viscous deformation due to ice loading changes between 1892 – 1992 on predicted relative sea level, crustal motion and geoid height during the 25-year record time frame.

Here we briefly assess the impact of extending the length of our modern ice history from 25 to 125 years on GIA predictions for simulations adopting the REG_P viscosity model. The greatest discrepancies between relative sea level and geoid height change predictions between simulations

adopting ICE-125 and ICE-25 are concentrated near the grounding line across the PSK and TG regions (Fig. S7), where the greatest ice loading changes occur prior to 1992 (Fig. 2a). Indicative of an ongoing viscous contribution from ice mass changes between 1892-1992, up to 11.3 cm greater sea level fall (~50% of total signal with ICE-125) and 2.5 mm difference in predicted geoid height change (~8% of the total signal with ICE-125) are found in simulations adopting ICE-125 versus ICE-25 model between 1992 and 2017 (Fig. S7a, d). Regardless of the adopted viscosity model, vertical crustal motion rates computed at the end of the ICE-125 ice history are greater in magnitude (up to ~2.8 mm/year) compared to those computed with the ICE-25 ice history (Fig. S7b, S8a). Discrepancies between horizontal crustal motions rates in simulations adopting ICE-125 versus ICE-25 are more spatially variable, with notable differences found adjacent to the grounding line (Fig. S7c, S8b). While the viscous contribution to GIA predictions from ice mass changes between 1892 – 1992 is notable throughout much of the TG and PIG basins, the contribution becomes negligible ~500 km inland of the modern-day grounding line.

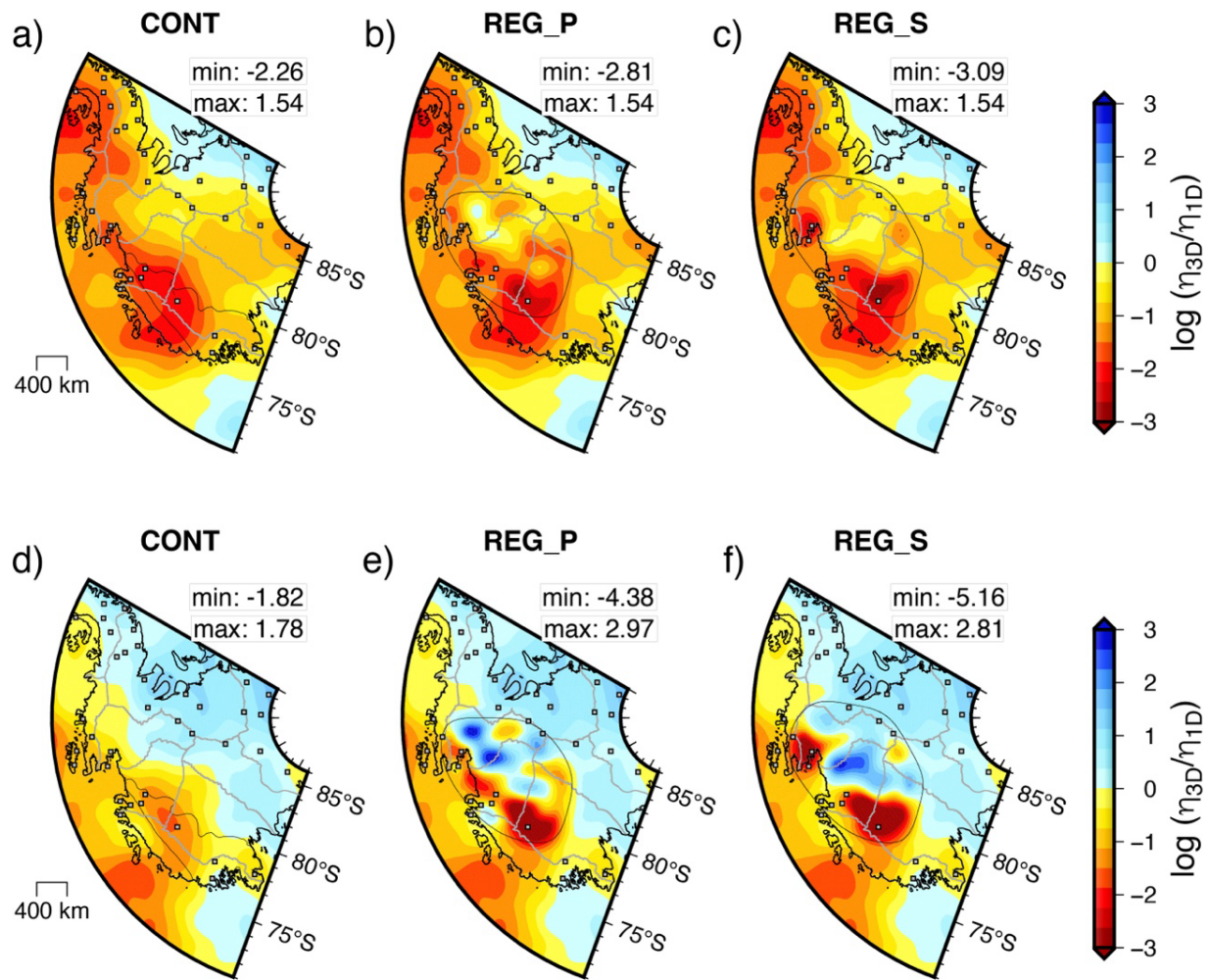


Figure S1. Depth slices through 3-D viscosity models at (a-c) 100 km depth and (d-f) 200 km depth. Depth slices are plotted as logarithmic viscosity perturbation maps like in Figure 1. The location of the maps are outlined in Fig. 1b.

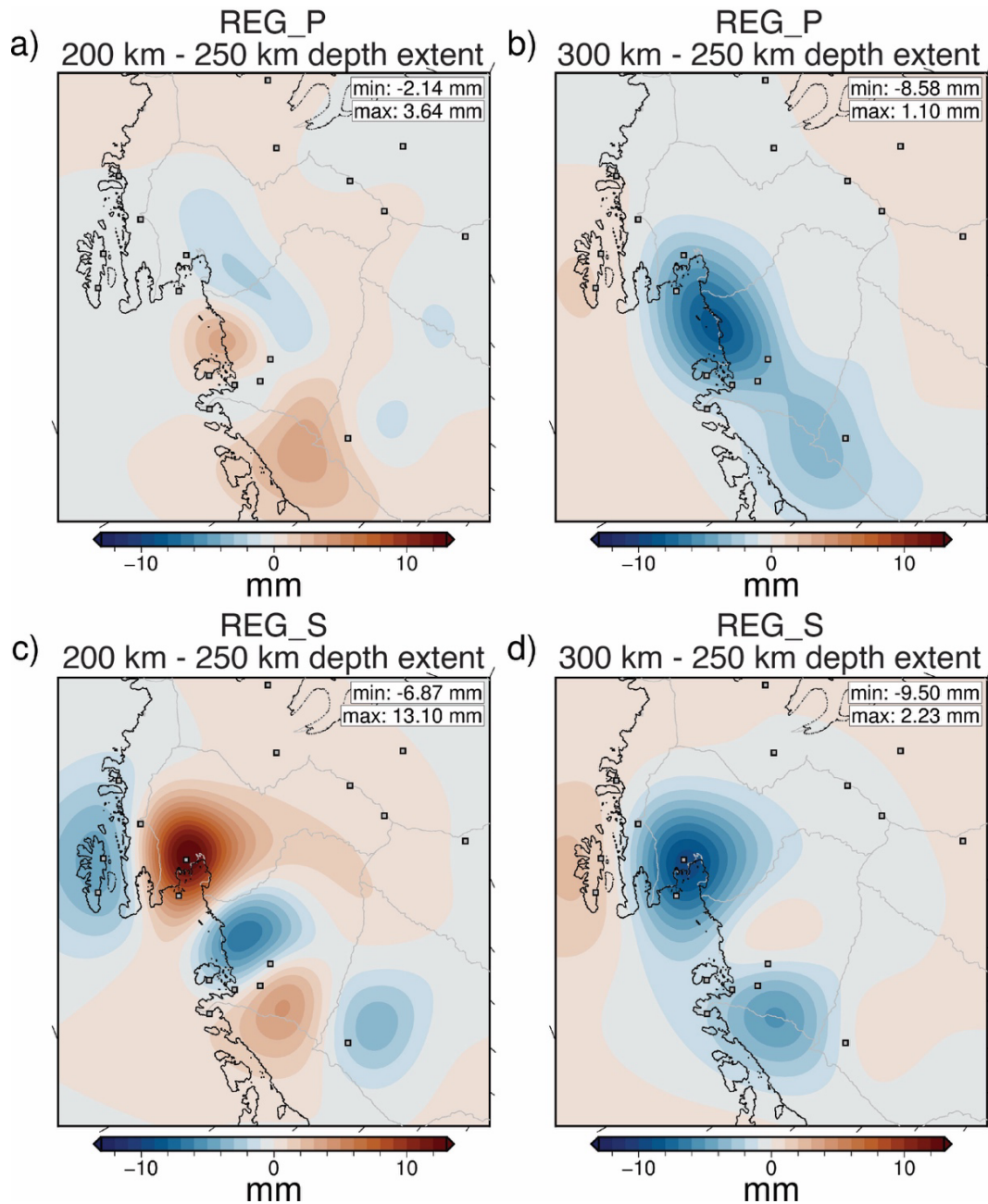


Figure S2. Difference in relative sea level predicted in simulations with ICE-25 for Earth models in which the regional body-wave tomography models were inserted in the ANT-20 and GLAD-M25 composite models over different depth extents (i.e., P- and S-wave models inserted to 200 km, 250 km, and 300 km depths). Note, the regional body wave model is inserted from the base of the lithosphere to 250 km depth for the REG_P and REG_S viscosity models. (a-b) Difference in predicted relative sea level between simulations adopting viscosity models where the P-wave model extends to (a) 200 km depth and (b) 300 km depth and the REG_P viscosity model. (c-d) Difference in predicted relative sea level between simulations adopting viscosity models where the S-wave model extends to (a) 200 km depth and (b) 300 km depth and the REG_S viscosity model.

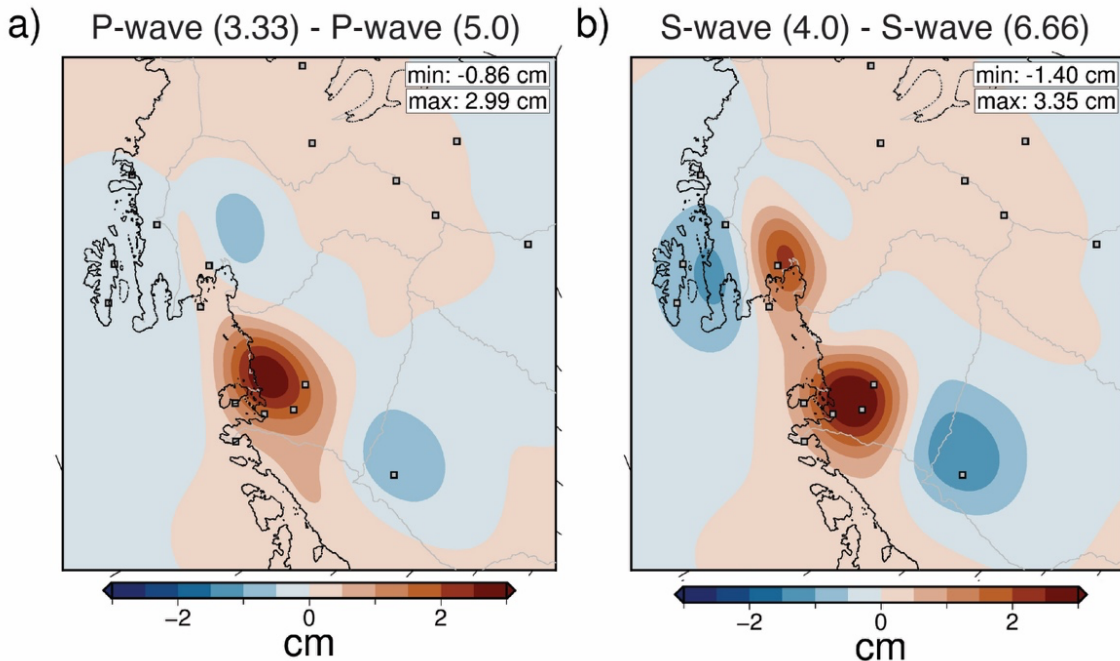


Figure S3. Impact of assumptions made in the construction of regional viscosity models on relative sea level predictions: (a) Difference in predicted relative sea level for simulations adopting a viscosity model constructed assuming high-end amplitude recovery in the P-wave model (i.e., 30% amplitude recovery) and the REG_P viscosity model. (b) Difference in predicted relative sea level for simulations adopting a viscosity model constructed assuming high-end amplitude recovery in the S-wave model (i.e., 25% amplitude recovery) and the REG_S viscosity model. All simulations shown here adopt the ICE-25 ice history. From this comparison, we find a maximum difference of 2.99 cm and 3.35 cm between relative sea level predictions adopting the viscosity models constructed accounting for high-end and low-end amplitude in the P-wave and S-wave models, respectively. Therefore, the adopted amplitude scaling factor only contributes up to $\sim 7\%$ of the total relative sea level prediction. Although there is some discrepancy in the predicted magnitude of relative sea level, a similar spatial pattern in relative sea level predictions is produced in simulation adopting the low- and high-end P- and S-wave models, respectively. The similarity in the spatial pattern of GIA predictions between models scaled for high- and low-end amplitude recovery indicates that the adopted scaling factor does not have the largest control on model predictions; instead, the spatial pattern of upper mantle viscosity has the greater impact on GIA predictions. Therefore, given the relatively minor impact of chosen amplitude scaling factor on GIA model predictions, we will focus on simulations adopting the REG_P and REG_S viscosity models throughout the main text.

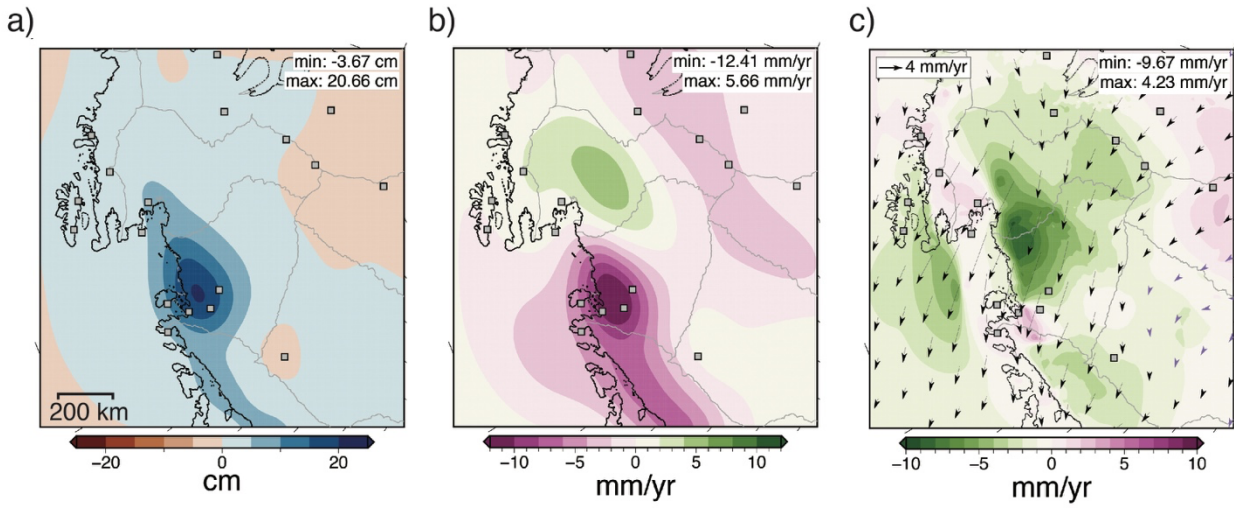


Figure S4. Difference in (a) relative sea level, (b) vertical crustal motion, and (c) horizontal crustal motion predictions between simulations adopting the 1D_WAIS viscosity model and the CONT viscosity model (1D_WAIS predictions minus CONT predictions) with the ICE-125 ice model.

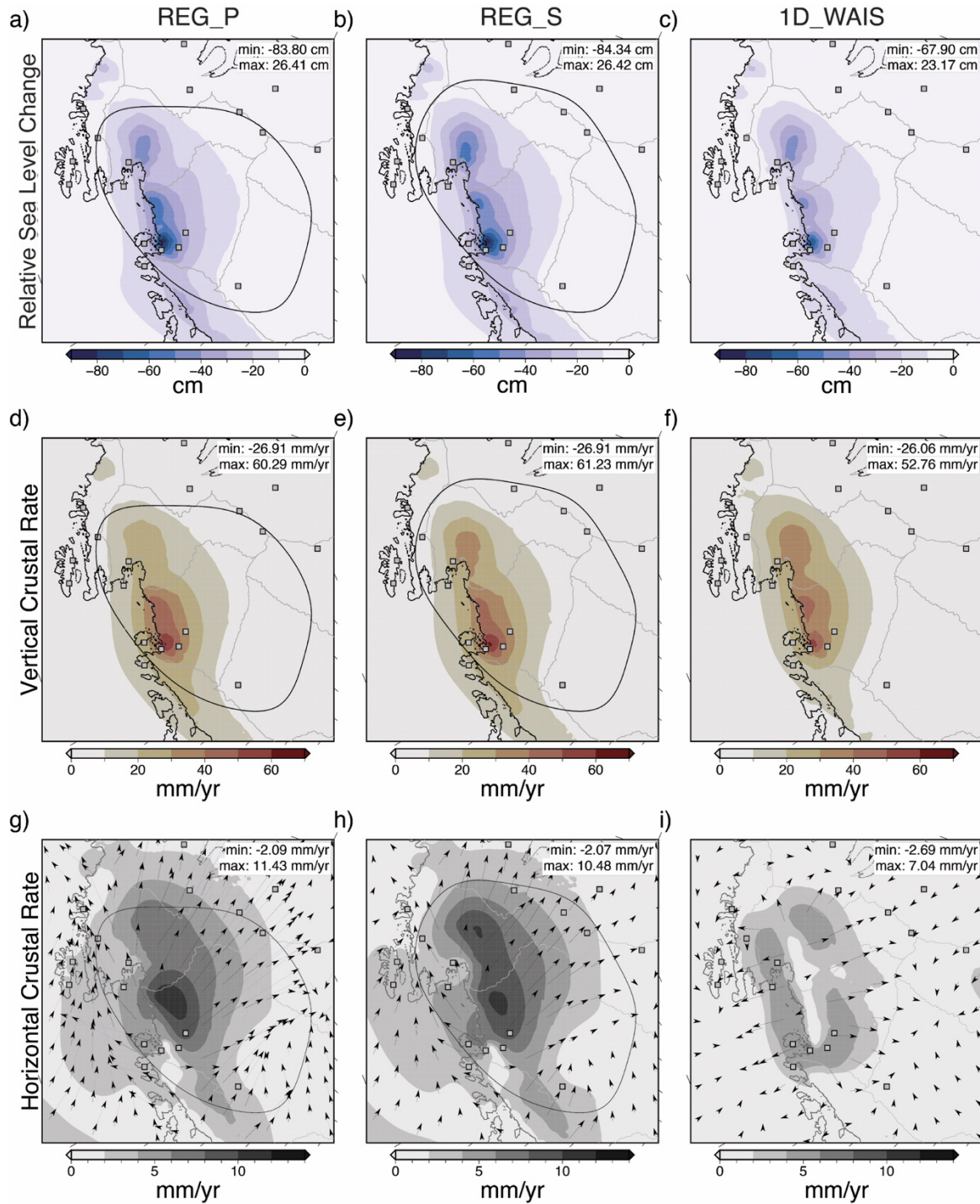


Figure S5. (a-c) Relative sea level predictions for simulations adopting the ICE-125 ice model and the (a) REG_P, (b) REG_S, and (c) 1D_WAIS viscosity models. (d-f) Vertical crustal motion rates predicted at the end of simulations adopting the ICE-125 ice model and the (d) REG_P, (e) REG_S, and (f) 1D_WAIS viscosity models. (g-i) Horizontal crustal motion rates predicted at the end of simulations adopting the ICE-125 ice model and the (g) REG_P, (h) REG_S, and (i) 1D_WAIS viscosity models.

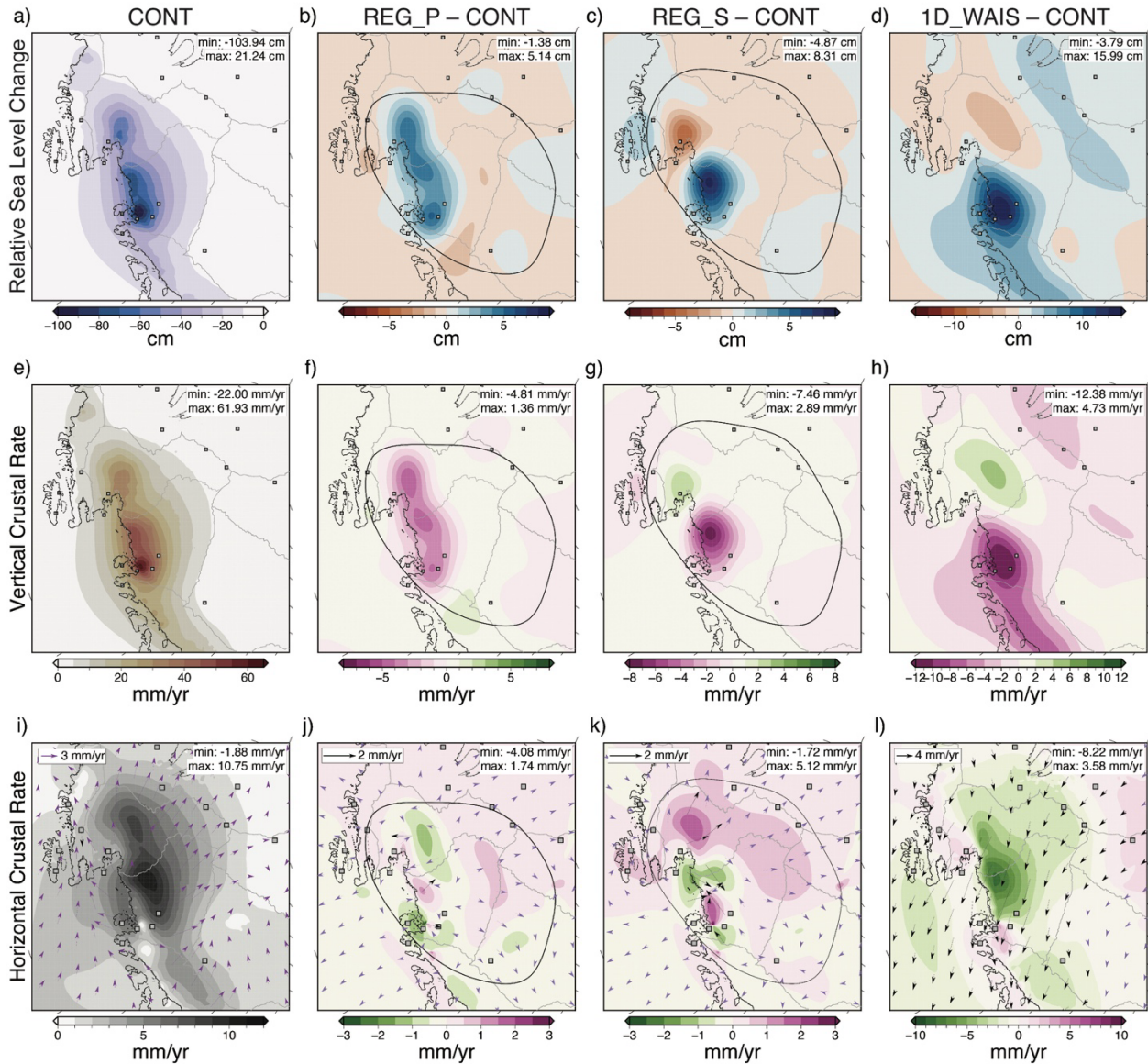


Figure S6. Influence of regional upper mantle structure on predictions of sea level and crustal motion rates for modern ice loading (ICE-25). (a) Relative sea level change in centimeters for a GIA model simulation with the CONT viscosity model and the ICE-25 ice model. (b-d) Difference in predicted relative sea level change between the (b) REG_P, (c) REG_S, (d) 1D_WAIS and CONT viscosity models. (e) Vertical crustal motion rate predicted at the end of a simulation adopting the CONT viscosity model and the ICE-25 model. (f-h) Difference in predicted vertical crustal motion rates between the (f) REG_P, (g) REG_S, and (h) 1D_WAIS viscosity models and the CONT viscosity model at the end of simulations with the ICE-25 ice model. (i) Horizontal crustal motion rate predicted at the end of the simulation adopting the CONT viscosity model and the ICE-25 ice model. (j-l) Difference in horizontal crustal motion rates after 25 years of loading (ICE-25) between the (j) REG_P, (k) REG_S, and (l) 1D_WAIS and CONT viscosity models. (j-l) Vectors show the difference in predicted direction and magnitude of horizontal crustal motion rates between the respective panel's viscosity model and the CONT viscosity model. Black and purple arrows correspond to locations with horizontal crustal motion rates ≥ 1 mm/year and < 1 mm/year, respectively.

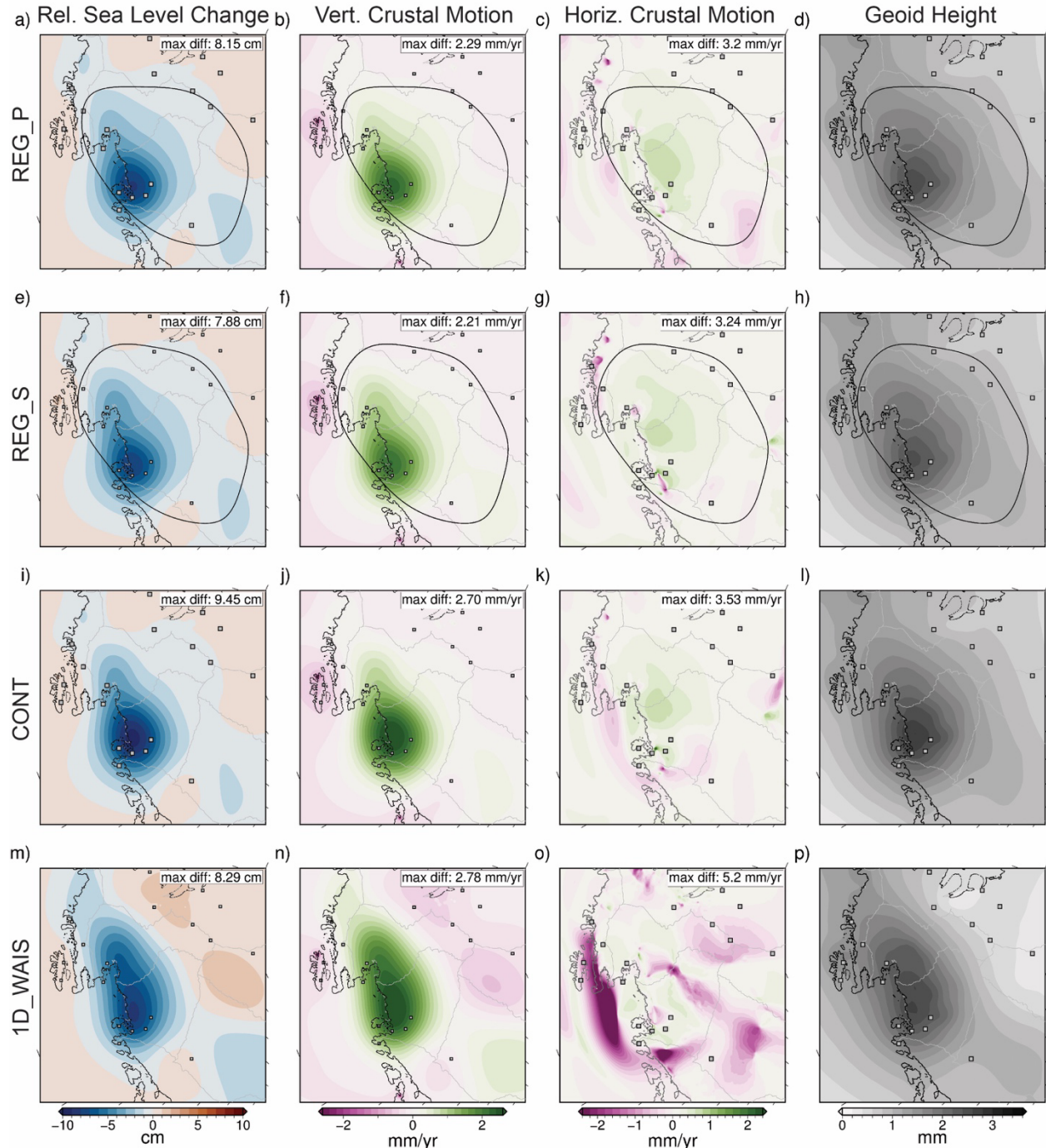


Figure S7. Impact of ice history length (ICE-125 versus ICE-25) on model predictions for the (a-d) REG_P, (e-h) REG_S, (i-l) CONT, and (m-p) 1D_WAIS viscosity models. Differences in relative sea level predictions for 1992-2017 are shown in the first column. Differences in vertical and horizontal crustal motion predictions at the end of the simulation in 2017 are in the second and third columns. Differences in geoid height predictions for 1992 – 2017 are in the fourth column. Extent of maps shown in all panels are the same as the inset in Figure 2a.

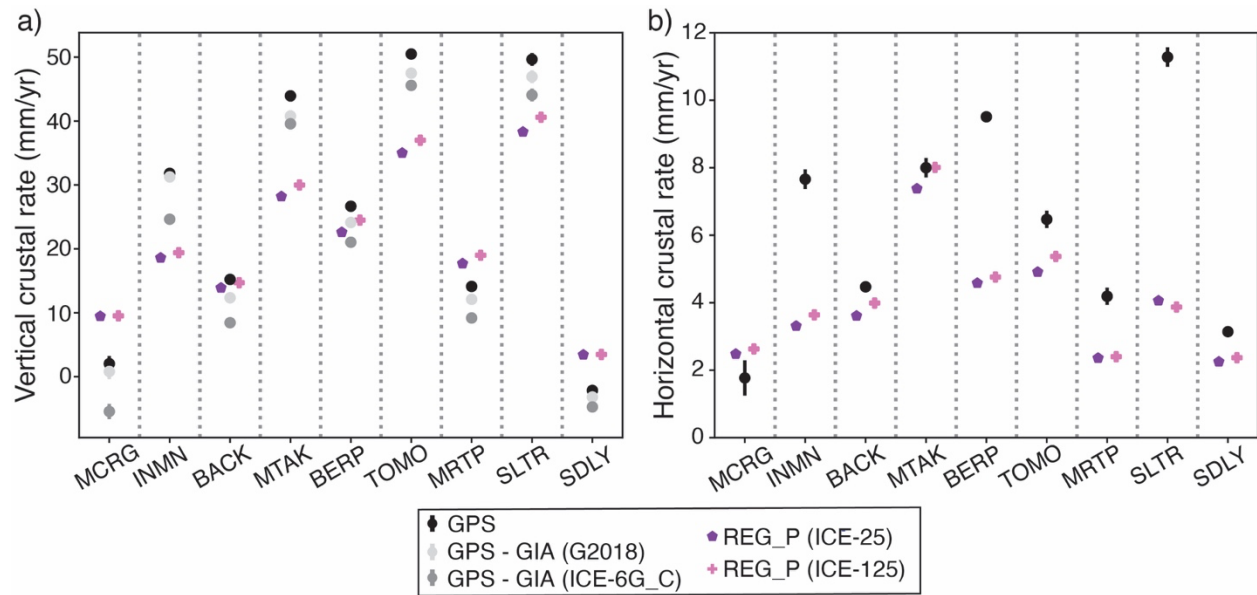


Figure S8. Comparison between predicted and observed crustal rates for simulations adopting ICE-125 and ICE-25. (a) Vertical and (b) horizontal crustal rates observed at select GPS sites located throughout central West Antarctica plotted with predicted crustal rates from simulations adopting either the ICE-25 or ICE-125 ice models with the REG_P viscosity model. Like in Fig. 6, observed vertical crustal rates are corrected based on the predictions from the Gomez et al. (2018) (abbreviated G2018 in the legend) and ICE-6G_C (Peltier et al., 2015) models.

Table S1. Observed and predicted crustal rates at GPS sites

			Observed						
			Vertical (mm/yr)	Horizontal (mm/yr)			Vertical Error (mm/yr)	Horiz. Error (mm/yr)	
Station	Latitude	Longitude		East	North	Total		Sigma E	Sigma N
BACK	-74.43044137	-102.4781855	15.22	0.21	4.47	4.47	0.11	0.04	0.03
BERP	-74.54593593	-111.8845842	26.67	1.22	9.43	9.51	0.12	0.06	0.05
INMN	-74.82086547	-98.88046683	31.81	-2.55	7.22	7.66	0.38	0.2	0.21
MCRG	-73.66779881	-94.64632176	2.03	-1.09	1.4	1.77	1.2	0.38	0.36
M RTP	-74.18040529	-115.1021358	14.12	0.4	4.17	4.19	0.57	0.2	0.16
MTAK	-	-	-	-	-	-	-	-	-
MTAK	76.315041329	-112.800012	43.94	-2.38	-7.64	8	0.89	0.21	0.2
SDLY	-77.13531279	-125.9745777	-2.15	2.78	1.46	3.14	0.17	0.03	0.05
SLTR	-75.09815674	-113.8795515	49.65	-3.23	10.8	11.28	1	0.21	0.2
TOMO	-75.80186751	-114.6619037	50.49	-5.86	-2.74	6.47	0.46	0.16	0.2
Predicted									
REG P, ICE-125									
REG P, ICE-25									
REG S, ICE-125									
CONT, ICE-125									
Station	Vertical (mm/yr)	Horizontal (mm/yr)			Vertical (mm/yr)	Horizontal (mm/yr)			
		East	North	Total		East	North	Total	
BACK	14.69	3.87	0.98	3.99	13.88	3.47	1.01	3.61	
BERP	24.53	3.12	3.59	4.76	22.58	2.89	3.55	4.58	
INMN	19.39	3.56	0.71	3.64	18.62	3.21	0.81	3.31	
MCRG	9.52	2.48	0.87	2.63	9.45	2.33	0.83	2.48	
M RTP	18.95	1.28	2.03	2.4	17.7	1.27	1.98	2.36	
MTAK	30.04	1.82	-7.81	8.01	28.2	1.66	-7.19	7.38	
SDLY	3.48	0.78	-2.23	2.37	3.43	0.69	-2.14	2.25	
SLTR	40.55	-0.41	3.85	3.87	38.34	-0.43	4.03	4.06	
TOMO	37.02	-1.53	-5.15	5.37	35.03	-1.48	-4.69	4.91	
BACK	16.09	3.58	0.96	3.71	15.17	3.93	1.38	4.16	
BERP	24.4	4.04	3.57	5.39	25.93	3.39	4.49	5.63	
INMN	24.04	3.11	0.78	3.21	21.44	3.25	1.48	3.57	
MCRG	8.76	2.37	0.46	2.42	9.22	2.18	0.56	2.25	
M RTP	19.32	1.52	2.32	2.78	19.54	1.14	2.5	2.75	
MTAK	30.35	3.30	-7.56	8.25	32.85	1.71	-8.06	8.24	
SDLY	2.83	1.24	-2.19	2.51	3.03	1.29	-2.1	2.46	

SLTR	41.58	1.21	4.26	4.43		43.76	-0.08	4.81	4.81
TOMO	38.64	-0.14	-5.10	5.1		40.57	-1.71	-5.37	5.63
1D WAIS, ICE-125									
	Vertical (mm/yr)	Horizontal (mm/yr)							
Station		East	North	Total					
BACK	15.3	-0.29	3.92	4.33					
BERP	20.05	0.07	4.77	5.2					
INMN	22.54	-0.9	4.4	4.8					
MCRG	11.08	-0.26	2.35	2.58					
M RTP	15.26	-1.2	3.2	3.75					
MTAK	24.72	-2.11	-3.77	4.78					
SDLY	3.11	-0.11	-0.76	0.66					
SLTR	34.22	-2.74	5.02	6.01					
TOMO	29.99	-4.09	-2.83	5.44					

References

- Antolik, M., Gu, Y. J., Ekström, G., and Dziewonski, A. M.: J362D28: a new joint model of compressional and shear velocity in the Earth's mantle, *Geophys. J. Int.*, 153, 443–466, <https://doi.org/10.1046/j.1365-246X.2003.01910.x>, 2003.
- Barletta, V. R., Bevis, M., Smith, B. E., Wilson, T., Brown, A., Bordoni, A., Willis, M., Khan, S. A., Rovira-Navarro, M., Dalziel, I., Smalley, R., Jr., Kendrick, E., Konfal, S., Caccamise 2nd, D. J., Aster, R. C., Nyblade, A., and Wiens, D. A.: Observed rapid bedrock uplift in Amundsen Sea Embayment promotes ice-sheet stability, *Science*, 360, 1335–1339, <https://doi.org/10.1126/science.aao1447>, 2018.
- Gomez, N., Latychev, K., and Pollard, D.: A coupled ice sheet–sea level model incorporating 3D earth structure: variations in Antarctica during the last deglacial retreat, *J. Climate*, 31, 4041–4054, <https://doi.org/10.1175/JCLI-D-17-0352.1>, 2018.
- Hay, C. C., Lau, H. C., Gomez, N., Austermann, J., Powell, E., Mitrovica, J. X., Latychev, K., and Wiens, D. A.: Sea level fingerprints in a region of complex Earth structure: The case of WAIS, *J. Climate*, 30, 1881–1892, <https://doi.org/10.1175/JCLI-D-16-0388.1>, 2017.
- Ivins, E. R., van der Wal, W., Wiens, D. A., Lloyd, A. J., and Caron, L.: Antarctic upper mantle rheology, *The Geochemistry and Geophysics of Antarctic Mantle*, *Memoirs*, vol. 56, edited by: Martin, A., and van der Wal, W., *Geol. Soc. Lond.*, 267–294, <https://doi.org/10.1144/M56-2020-19>, 2023.
- Kachuck, S. B., Martin, D. F., Bassis, J. N., and Price, S. F.: Rapid viscoelastic deformation slows marine ice sheet instability at Pine Island Glacier, *Geophys. Res. Lett.*, 47, e2019GL086446, <https://doi.org/10.1029/2019GL086446>, 2020.

Kustowski, B., Ekström, G., and Dziewonski, A.: Anisotropic shear-wave velocity structure of the Earth's mantle: A global model, *J. Geophys. Res.-Sol. Ea.*, 113, B06306, <https://doi.org/10.1029/2007JB005169>, 2008.

Lucas, E. M., Soto, D., Nyblade, A. A., Lloyd, A. J., Aster, R. C., Wiens, D. A., O'Donnell, J. P., Stuart, G. W., Wilson, T. J., Dalziel, I. W., and Winberry, J. P.: P-and S-wave velocity structure of central West Antarctica: implications for the tectonic evolution of the West Antarctic Rift System, *Earth Planet. Sc. Lett.*, 85, 116437, <https://doi.org/10.1016/j.epsl.2020.116437>, 2020.

Nield, G. A., Barletta, V. R., Bordoni, A., King, M. A., Whitehouse, P. L., Clarke, P. J., Domack, E., Scambos, T. A., and Berthier, E.: Rapid bedrock uplift in the Antarctic Peninsula explained by viscoelastic response to recent ice unloading, *Earth Planet. Sc. Lett.*, 397, 32–41, <https://doi.org/10.1016/j.epsl.2014.04.019>, 2014.

Peltier, W., Argus, D. F., and Drummond, R.: Space geodesy constrains ice age terminal deglaciation: The global ICE-6G_C (VM5a) model, *J. Geophys. Res.-Sol. Ea.*, 120, 450–487, <https://doi.org/10.1002/2014JB011176>, 2015.

Powell, E., Gomez, N., Hay, C., Latychev, K., and Mitrovica, J.: Viscous effects in the solid Earth response to modern Antarctic ice mass flux: Implications for geodetic studies of WAIS stability in a warming world, *J. Climate*, 33, 443–459, <https://doi.org/10.1175/JCLI-D-19-0479.1>, 2020.

Powell, E., Latychev, K., Gomez, N., and Mitrovica, J. X.: The robustness of geodetically-derived 1-D Antarctic viscosity models in the presence of complex 3-D viscoelastic Earth structure, *Geophys. J. Int.*, 231, ggac129, <https://doi.org/10.1093/gji/ggac129>, 2022.

Wan, J. X. W., Gomez, N., Latychev, K., and Han, H. K.: Resolving glacial isostatic adjustment (GIA) in response to modern and future ice loss at marine grounding lines in West Antarctica, *The Cryosphere*, 16, 2203–2223, <https://doi.org/10.5194/tc-16-2203-2022>, 2022.